Size-Dependent Spectroscopy of InP Quantum Dots

O. I. Micić,* H. M. Cheong, H. Fu,† A. Zunger,*,† J. R. Sprague, A. Mascarenhas, and A. J. Nozik*

National Renewable Energy Laboratory, 1617 Cole Boulevard, Golden, Colorado 80401

Received: February 6, 1997; In Final Form: April 11, 1997[⊗]

The spectroscopic behavior of colloidal InP quantum dots (QDs) has been investigated as a function of the mean QD diameter (which ranged from 26 to 60 Å). Absorption spectra show up to three peaks or shoulders which reflect excited state transitions in the QDs. Global photoluminescence (PL) spectra (excitation well to the blue of the absorption onset and which consequently excites most of the QDs in the size distribution) show broad PL emission. The emission and absorption features shift to higher energy with decreasing QD size. Resonant PL spectra (size-selective excitation into the tail of the absorption onset) show increasing fluorescence line narrowing with increasing excitation wavelength; PL and photoluminescence excitation spectroscopy were used to derive the PL red shift as a function of QD size. The resonant red shifts for QDs of a single size were extracted from PL data that reflect the emission from an ensemble of QD diameters. An analysis of the single-dot resonant red shift (difference between PL peak and the first absorption peak) as a function of the single QD diameter indicate that the results are consistent with a model in which the emission occurs from an intrinsic, spin-forbidden state, split from its singlet counterpart, due to screened electron-hole exchange.

I. Introduction

The spectroscopic properties of semiconductor quantum dots (QDs) are under extensive study because such data provide critical information on the electronic energy level structure of the QDs. A major current issue is the relative importance of the QD surface compared to the QD core structure in controlling the photoluminescence (PL) properties of QDs. In early investigations,[1−7] the predominant view was that the surface structure, especially surface defects, controlled the PL properties; this view was generally accepted because of (i) the exceedingly high surface to volume ratios that are present in small-sized QDs (30% of the atoms in a 35 Å diameter III−V QD are at the surface); (ii) the rather low quantum yield and its dependence on the passivation agent, and (iii) the evidence[6] that at least in Si particles, the red emission involves surface defects. However, recent work[8−14] on CdSe QDs has suggested that at least the near-edge emission in selective excitation experiments is determined by the QD core structure, not the surface structure. One important basis for this conclusion were measurements of the near-band-edge PL red shift as a function of QD size;[8−14] the origin of this red shift was attributed to an enhanced electron-hole exchange interaction in QDs with strong confinement.[8−14] The uncertainty about the relative roles of surface *vs* core in determining the overall QDs electronic structure stems, in part, from the lack of theoretical modeling of the QD surface, as all standard models of QDs[9,11−13] assume an infinite potential barrier at the QDs boundary, thus excluding surface states. However a recent explicit model of the InP quantum dot surface[15] showed how surface vacancies introduce states in the QD band gap, and how these states hybridize and shift the QD band-edge states, affecting radiative lifetimes and quantum yields.

In the present work we focus on the optical properties of excellent quality InP QDs synthesized by colloidal chemistry,[16−19] including measurements of the PL red shift and lifetimes. We have reported previously[18] that surface defects that are present after the initial formation of the QDs can be passivated by treating the InP QDs with dilute HF. This treatment yields exceptionally high quality InP QDs in which deep red-shifted PL emission (peaking at about 850 nm for 30 Å diameter QDs (band gap of 2.3 eV) and attributed to surface traps formed in the initial QD synthesis) is completely removed. Consequently, the emission from our HF-treated InP QDs consists only of a single, but broad, PL peak near the absorption edge of the sample; the quantum yield of this near-band-edge emission is very high (60% at 10 K and 30% at room temperature).[18]

InP QDs prepared by colloidal chemistry generally exhibit a significant size distribution that depends upon the synthesis conditions and post-synthesis treatments. Our InP QD samples have a size distribution of about 10% around their mean diameter; the mean diameters reported here range from about 25 to 60 Å. The finite QD size distribution broadens (inhomogeneous line broadening) and complicates their optical emission and absorption spectra. One strategy to ameliorate the problem of the size distribution and inhomogeneous line broadening is to perform size-selective spectroscopy and to subject the results to an analysis that distills from the data the effective single-dot emission. Size-selective PL emission is obtained by restricting the excitation wavelength to the onset region of the absorption spectrum (the long wavelength tail of the spectrum); thus, only particles larger than a given size in the distribution are excited. This technique is termed fluorescence line narrowing (FLN)—the resulting PL spectra being considerably narrowed. Another related technique is to perform photoluminescence excitation spectroscopy (PLE), in which the intensity of a selected emission wavelength is controlled and the excitation wavelengths are scanned to produce the PLE spectrum. The results of these two techniques can be combined to determine the red shift of the near band-edge emission as a function of excitation energy. Because the size-selective FLN and PLE spectroscopic techniques still sample a residual, significant size distribution of QDs, we have developed an analysis that extracts the red shift for single dots as a function

† Solid State Theory Group.

[⊗] Abstract published in *Advance ACS Abstracts,* May 15, 1997.

S1089-5647(97)00473-2 CCC: $14.00

of their diameter from the FLN and PLE data that are generated from a distribution of QD sizes.

II. Experimental Section

A. QD Synthesis. Colloidal InP QDs were produced by the following procedure: first, indium oxalate (1.15 g), tris-(trimethylsilyl)phosphine (0.75 g), and a colloidal stabilizer (10 g of a mixture of trioctylphosphine oxide (TOPO) and trioctylphosphine (TOP) in a TOPO:TOP ratio of 0.1:1, were mixed together at room temperature to form a transparent solution of an InP precursor; then, the precursor solution was heated at 250−300 C for 3 days. This procedure produces a colloidal solution of InP QDs that are capped with TOPO/TOP. The TOPO/TOP cap can be replaced with other stabilizers, such as thiols, furan, fatty acids, sulfonic acids, and amines. The QDs can be isolated as a powder by precipitation with methanol; the resultant QD powders can be readily redissolved in nonpolar solvents (such as toulene or a hexane−butanol mixture) to reform transparent colloidal QD dispersions. Fractionation of the QD particles into different sizes can be obtained by selective precipitation methods.[20] X-ray data show that the QD particles have zincblende crystal structure; TEM and electron diffraction data were also consistent with the zincblende InP structure. However, the TEM results were not sufficient to provide detailed information about the specific shape of the QD particles, nor their shape distribution.

Intense band-edge emission from our InP QDs can be achieved after etching the particles with a dilute butanolic solution of HF or NH_4F;[18] 50 μL of the butanolic solution, which contains 5% HF and 10% H_2O, is added to 1 mL of a colloidal solution of InP QDs. The InP colloid contains 0.5 mg InP/mL of toluene solution that also contains polyvinyl butyral (75 mg PVB/mL toluene). After etching is complete (typically, 20 h), this solution can be deposited on a sapphire substrate and dried to yield a stable QD film. Alternatively, after etching, the QDs can be treated with octanethiol, and the QDs (now capped with octanethiol) can be redissolved in tetrahydrofuran to produce a colloidal QD solution that is stable in air and which shows intense band-edge emission after a month in contact with air. After the etching process, the PL intensity increases by a factor of ten, and the near infrared emission produced by deep surface traps is completely removed.[18] The near-band-edge quantum yield increase from 30% to 60% as the temperature decreases from 300 to 10 K.[18]

B. Spectroscopy. The FLN and PLE measurements were performed at 11 K in a closed-cycle He cryostat, using either the 5145-Å line of an Ar ion laser or a dye laser with a DCM-special dye (1.80−2.05 eV) as the excitation source. The intensity of the excitation was ∼3 mW at the sample; the beam was focused by a cylindrical lens to a spot size of ∼5 mm × 100 μm. The luminescence signal was dispersed by a Spex 0.85-m double monochromator and detected by a cooled GaAs photomultiplier tube with photon-counting electronics. The spectral resolution was ∼0.3 meV. Room temperature measurements of the PL spectra were obtained with a SPEX Fluorolog-2, spectrofluorimeter. Absorption spectra were obtained with a CARY 5 spectrometer.

PL lifetimes were obtained using conventional time-correlated single photon counting techniques. A cavity-dumped synchronously-pumped dye laser (Spectra-Physics 3500) operating at 580−620 nm provided pump pulses of 10 ps. A Hamamatsu microchannel plate detector provided a typical instrument response function of 70 ps. The lifetimes were determined using a three-component exponential fit to the decay data.

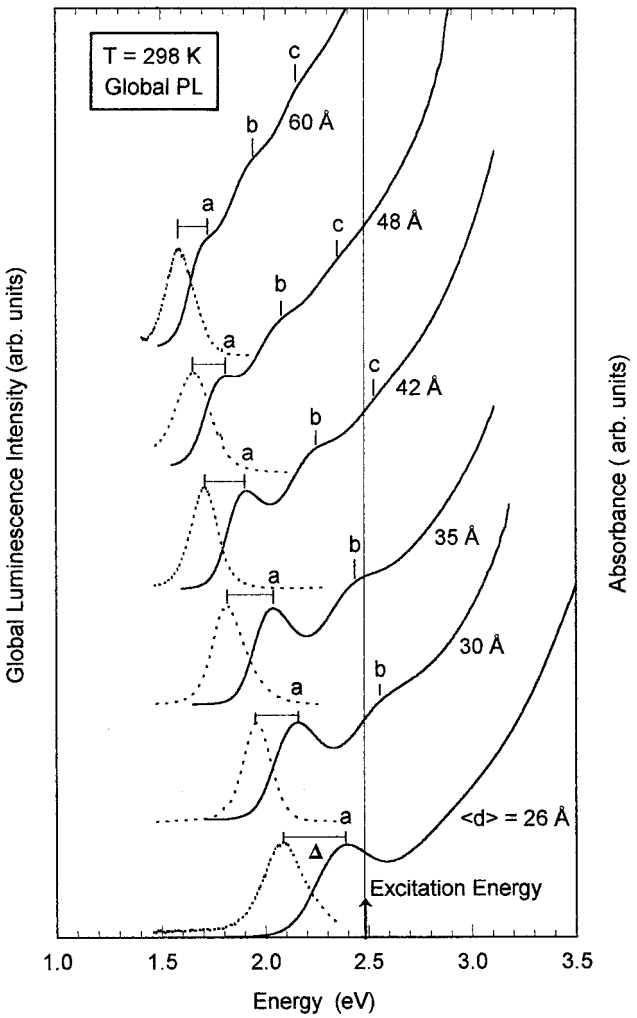

Figure 1. Absorption (solid line) and global PL (dotted line) spectra at 298 K for colloidal ensembles of InP QDs with different mean diameters. All QD colloidal samples were photoexcited at 2.48 eV.

III. Results

A. Global Photoluminescence. Global PL from the InP QD samples is defined as the PL that is observed when the excitation energy is much higher than the energy of the absorption threshold exhibited in the absorption spectrum produced by the ensemble of QDs in the sample. That is, the excitation wavelength is well to the blue of the first absorption peak for the QD ensemble, and therefore a large fraction of all the QDs in the sample are excited. The particle diameters that are excited range from the largest in the ensemble to the smallest which has a diameter that produces a blue-shifted band gap equal to the energy of the exciting photons.

On the other hand, if the excitation energy is restricted to the onset region of the absorption spectrum of the QD ensemble, then a much narrower range of QD sizes is excited; these QDs will have the larger particle sizes in the ensemble. Consequently, the PL spectra from this type of excitation show narrower line widths and smaller red shifts with respect to the excitation energy. A detailed quantitative analysis of global PL viá a viś FLN is presented below.

Figure 1 shows typical room temperature absorption and global emission spectra of the InP colloids with mean particle diameters ranging from 26 to 60 Å as measured by TEM; the excitation energy for all QD sample ensembles in Figure 1 was 2.48 eV, well above their absorption onset in each case. The absorption spectra show one or more broad excitonic peaks

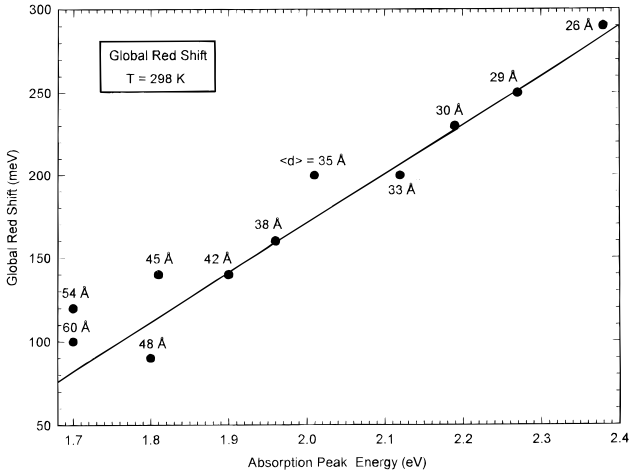

Figure 2. The global red shift for different colloidal ensembles of InP QDs as a function of the position of the first peak in their absorption spectra; the mean diameter of the QD ensemble is shown for each data point. The red shift is defined as the difference between the energies of the PL peak and the first absorption peak.

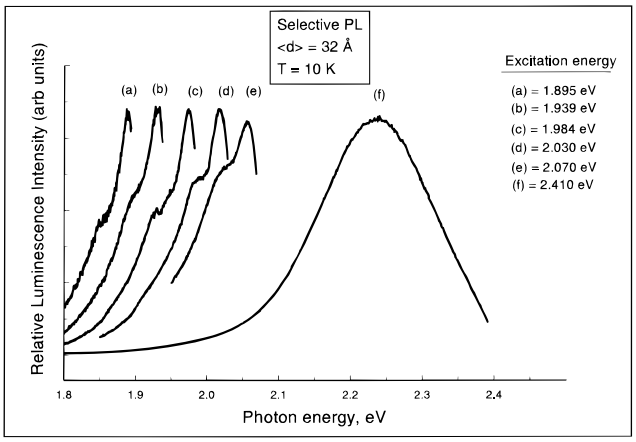

Figure 3. PL spectra at 10 K for an ensemble of InP QDs with a mean diameter of 32 Å for different excitation energies. The first absorption peak for this QD ensemble is at 2.17 eV, so that PL curves a−e result from excitation (1.895−2.070 eV) in the red tail of the onset region of the absorption spectrum and are FLN spectra; curve f is a global PL spectrum since its excitation was at 2.41 eV and is well to the blue of the first absorption peak.

which reflect substantial inhomogeneous line broadening arising from the QD size distribution; as expected the spectra shift to higher energy as the QD size decreases. The color of our InP QD samples changes from deep red (1.7 eV) to green (2.4 eV) as the diameter decreases from 60 to 26 Å. Bulk InP is black with a room-temperature band gap of 1.35 eV and an absorption onset at 918 nm. Higher energy transitions above the first excitonic peak in the absorption spectra can also be easily seen in QD samples with mean diameters equal to or greater than 30 Å. For QDs with diameters equal to or greater than 42 Å, a third transition can even be seen in the absorption spectra. The spread in QD diameters is generally about 10% and is somewhat narrower in samples with larger mean diameters; this is why higher energy transitions can be resolved for the larger-sized QD ensembles. All of our prepared QD nanocrystallites are in the strong confinement regime since the Bohr radius of bulk InP is about 100 Å.

The global emission peaks in Figure 1 show an increasing red shift from the first excitonic absorption peak as the mean QD size decreases from 60 to 26 Å; the results are summarized in Figure 2. The global ("nonresonant") red shift is as large as 300 meV for samples with the smallest mean diameter.

B. Size-Selected Photoluminescence (FLN and PLE Spectra). FLN spectra at 10 K are shown in Figure 3a−e for an InP QD sample ensemble with a mean diameter of 32 Å; FLN/PL spectra are shown for a series of excitation energies (1.895 to 2.07 eV) spanning the absorption tail near the onset of absorption for this sample. Also shown is the global PL spectrum produced when the excitation energy (2.41 eV) is deep into the high energy region of the absorption spectrum (Figure 3f).

FLN spectra can be combined with PLE spectra to determine the resonant red shift. The experiment is done as follows: (a) first, a photon energy is selected in the onset region of the absorption spectrum of the QD ensemble spectrum, and this energy is set as the detected photon energy in the PLE; (b) the PLE spectrum is then obtained, and the first peak of the PLE spectrum is taken to be the lowest energy excitonic transition for the QDs capable of emitting photons at the selected energy; (c) an FLN spectrum is then obtained with excitation at the first peak of the PLE spectrum. The energy difference between the first FLN peak and the first PLE peak is then defined as the resonant red shift for the ensemble of QDs represented by the selected PL excitation energy. This process is repeated across the red tail of the absorption onset region of the absorption spectrum to generate the resonant red shift as a function of QD size. Typical FLN and PLE spectra are shown in Figure 4 for InP QDs with a mean diameter of 32 Å. The resultant $T = 11$ K resonant red shift as a function of PL excitation energy is presented in Figure 5.

The above technique does not directly produce the *single-dot* resonant red shift as a function of QD size because the data still reflect the effects of a finite size distribution; in the next section the red shift for QDs of a single diameter are derived from the FLN and PLE data.

C. Extracting the Single-Dot Red Shift from the FLN/PLE Spectra. Conventional samples include dots of many sizes $\{d\}$, with a typical distribution

$$P(d,\langle d\rangle) = \frac{1}{\sqrt{2\pi}\sigma_d} e^{-(d-\langle d\rangle)^2/2\sigma_d^2} \tag{1}$$

about the average size $\langle d\rangle$. The distribution (1) is similar to the log-normal form selected in ref 16. The standard deviation σ_d can be deduced from high resolution TEM.[16] Because of the existence of a distribution of dots, each emitting at its own characteristic energy, the measured PL intensity represents an ensemble average, denoted here as $\bar{I}_{PL}(\epsilon, \epsilon_{excit}, \langle d\rangle)$ where ϵ_{excit} is the excitation energy. It is of interest to extract from the measured $\bar{I}_{PL}(\epsilon, \epsilon_{excit}, \langle d\rangle)$ *vs* ϵ_{excit} (Figure 5) the underlying single-dot red shift, for two reasons. (i) Theory[8,9,15,21] calculates single-dot quantities, not the ensemble average, and (ii) part of the observed ensemble red shift is due to the distribution effect, not to an intrinsic effect; it is of interest to separate these contributions.

To extract the single-dot red shift from the measured FLN, we simulate the ensemble emission intensity as

$$\bar{I}_{PL}(\epsilon, \epsilon_{excit}, \langle d\rangle) = \sum_{d > d_c(\epsilon_{excit})} \alpha(\epsilon_{excit}, d)\, I_{PL}(\epsilon, d)\, P(d, \langle d\rangle) \tag{2}$$

Here, $\alpha(\epsilon_{excit}, d)$ is the single-dot absorption coefficient at the energy $\epsilon_{excit} > E_g(d)$, where E_g is the excitonic band gap (arrows in Figure 5). The dot's emission energy is $E_g(d) - \Delta(d)$, where $\Delta(d)$ is the single-dot red shift that we

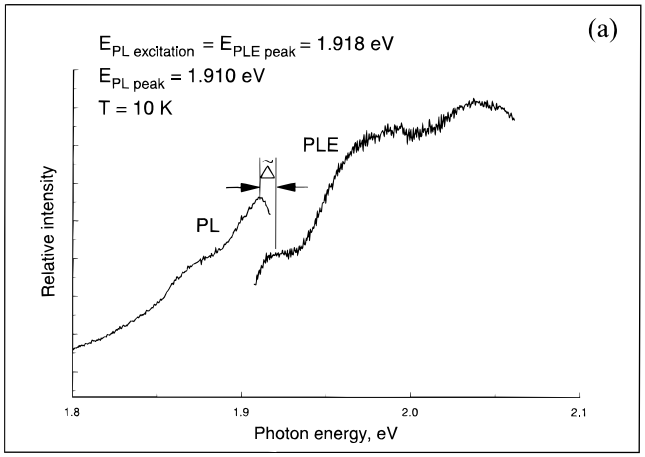

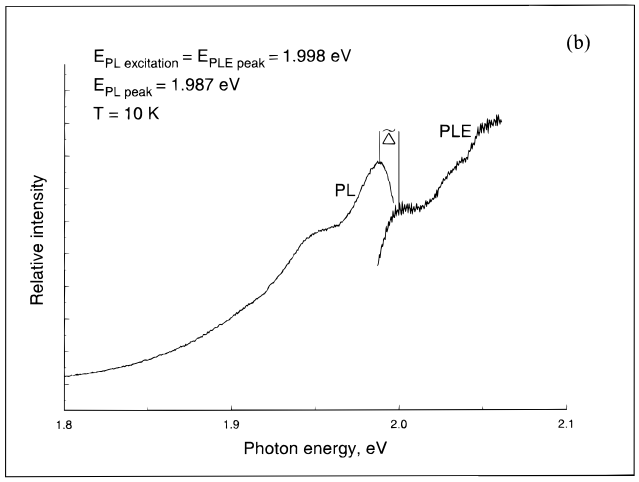

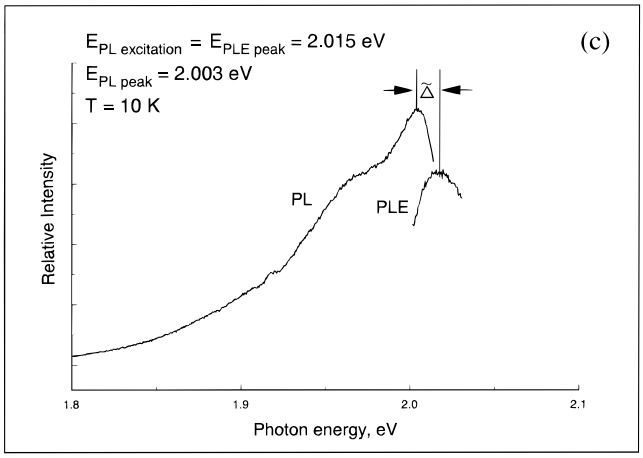

Figure 4. Representative pairs of PL (FLN) and PLE spectra for the InP ensemble with a mean diameter of 32 Å where the PLE spectra were obtained by scanning the PL detection across the onset region of the absorption spectrum of the QD ensemble, and the PL spectra were obtained by exciting at the energy of the first peak in the PLE spectra for the different PL detection energies. The resonant red or Stokes shift is defined as the energy difference between the PL peak and the first PLE peak.

wish to determine. The single-dot emission intensity is thus

$$I_{\mathrm{PL}}(\epsilon, d) = \frac{1}{\sqrt{2\pi}\sigma_{\mathrm{PL}}} e^{[\epsilon - (E_{\mathrm{g}}(d) - \Delta(d))]^2/2\sigma_{\mathrm{PL}}^2} \tag{3}$$

where σ_{PL} is the intrinsic broadening of the emission of a single dot, interacting in the ensemble with all other dots. The

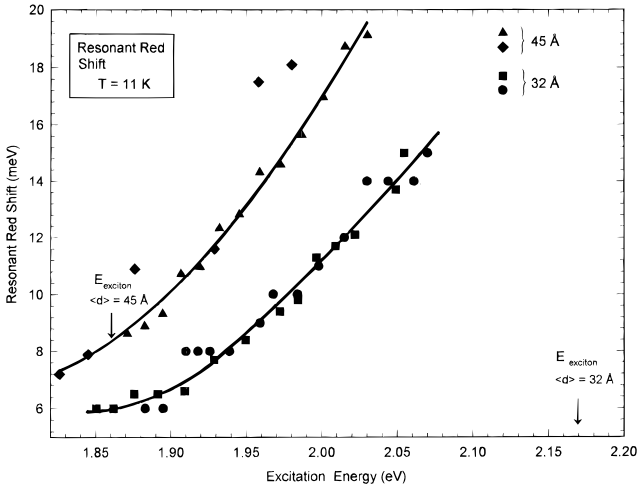

Figure 5. The red shift for InP QD ensembles at 10 K with mean diameters of 32 and 45 Å. The data for the 32 Å sample were obtained with excitation to the red of the first absorption peak (2.17 eV) and represent resonant Stokes shifts. For the 45 Å QD ensemble, the PL excitation was to the blue of their first absorption peak and show a larger red shift.

excitonic gap of a single dot is

$$E_{\mathrm{g}}(d) = E_{\mathrm{g}}(\infty) + \frac{A}{d^n} \tag{4}$$

where $E_{\mathrm{g}}(\infty)$ is the bulk band gap (1.45 eV for InP at $T = 10$ K or 1.35 at 300 K). For passivated InP dots,[21] $A = 55.2527$ and $n = 1.3611$. The single-dot red shift is taken in the form

$$\Delta(d) = \frac{B}{d^m} \tag{5}$$

where B and m are to be determined from our fit to experiment (see below). The sum over d in eq 2 is limited to those values satisfying $E_{\mathrm{g}}(d) < \epsilon_{\mathrm{excit}}$, so in effect $\epsilon_{\mathrm{excit}}$ in this equation depends on d.

We fitted the resonant red shift data of Figure 5 for $\langle d \rangle = 32$ Å, using $\sigma_{\mathrm{d}} = 2.5$ Å (the average of the TEM measured values of ref 18), $\sigma_{\mathrm{PL}} = 2$ meV, and taking α (ϵ,d) to be a constant, over the narrow range of excitation energies involved in Figure 5. Denoting the energy of the peak of the ensemble emission $\bar{I}_{\mathrm{PL}}(\epsilon, \epsilon_{\mathrm{excit}}, \langle d \rangle)$ as ϵ_{peak} ($\epsilon_{\mathrm{excit}}$, $\langle d \rangle$), we define the "ensemble red shift" as

$$\tilde{\Delta}(\epsilon_{\mathrm{excit}}, \langle d \rangle) = \epsilon_{\mathrm{peak}}(\epsilon_{\mathrm{excit}}, \langle d \rangle) - \epsilon_{\mathrm{excit}} \tag{6}$$

Figure 6 compares the measured (Figure 5) $\tilde{\Delta}$ *vs* $\epsilon_{\mathrm{excit}}$ (diamondlike symbols) to the simulated value (crosses) and shows good agreement. The best fit occurs at

$$\Delta_{\mathrm{exptl}}(d) = 9500/d^{1.96}\ (\mathrm{meV}) \tag{7}$$

although the fit is somewhat sensitive to the assumed σ_{PL} value. The single-dot red shift deduced from experiment (Δ_{exptl}) is shown as a solid line in Figure 6. This figure illustrates that the single-dot red shift $\Delta(\epsilon_{\mathrm{excit}})$ is smaller than the ensemble red shift $\tilde{\Delta}(\epsilon_{\mathrm{excit}})$ and has a different slope. Thus, if one is to compare measured red shifts to some microscopic theory,[8,9,11−13] it is important to first convert $\tilde{\Delta}$ to Δ.

Figure 7 shows the simulated ensemble emission spectra for different excitation energies: when $\epsilon_{\mathrm{excit}}$ is higher than all individual absorption thresholds (Figure 7a where $\epsilon_{\mathrm{excit}} = 2.64$ eV) one finds a "global", broad PL (compare Figure 3 trace f), while as $\epsilon_{\mathrm{excit}}$ (denoted as vertical arrows) is lowered, the

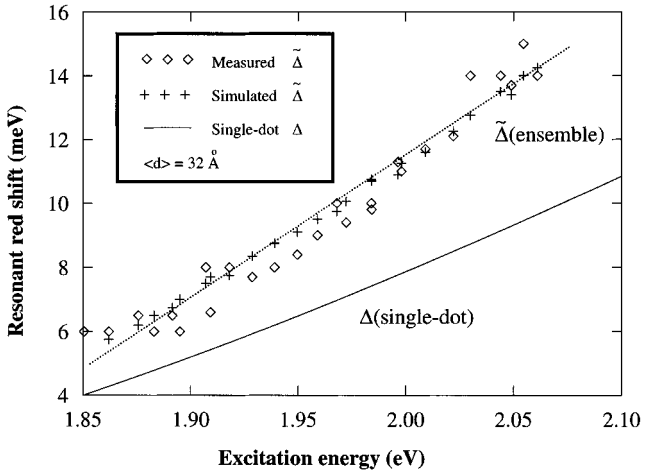

Figure 6. Measured (diamond shaped symbols) ensemble red shift $\tilde{\Delta}$ as a function of excitation energy for $\langle d\rangle = 32$ Å compared with the simulated results (plus signs) using $\sigma_{PL} = 2$ meV, $\sigma_d = 2.5$ Å, $E_g = 1.45 + 55.2527/d^{1.3611}$ and $\alpha(\epsilon, d) =$ const. The single-dot red shift deduced from the simulation (eq 7) is shown as a solid line.

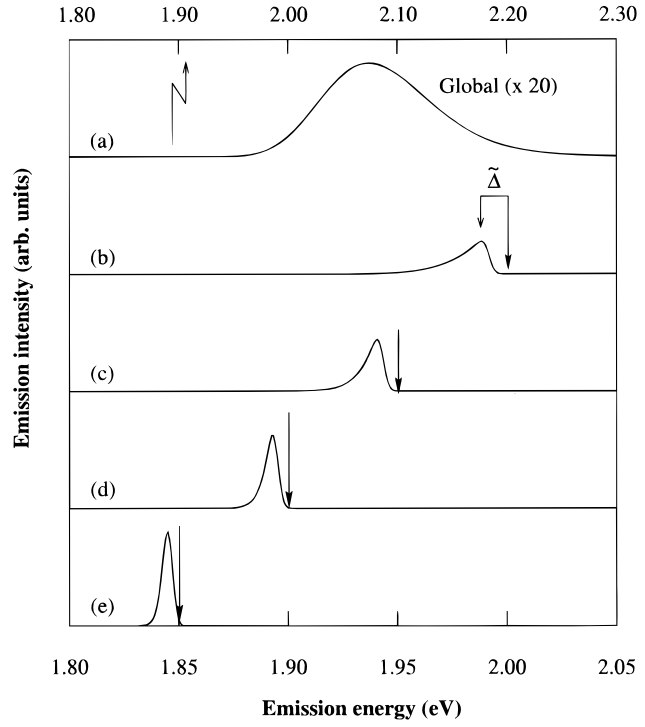

Figure 7. Simulated ensemble emission spectra $\bar{I}(\epsilon, \epsilon_{excit}\langle d\rangle)$ for a few values of excitation energies ϵ_{excit} shown as vertical arrows at $\langle d\rangle = 32$ Å, illustrating a "globe PL" (part a $\epsilon_{excit} = 2.64$ eV) and selectively excited PL (parts b−e). The ensemble red shift is illustrated in part b as the difference between peak emission energy and the excitation energy (eq 6).

emission narrows, shifts to the red, and has a lower $\tilde{\Delta}(\epsilon_{excit})$ (Figure 7b−e). These trends parallel the observations (Figures 3 and 4). The range of σ_{PL} used in our fit can be narrowed down significantly by requiring that the simulated (half) width of $\bar{I}_{PL}$ shown in Figure 7 agrees with experiment (Figures 3 and 4). This is satisfied at $\sigma_{PL} \cong 2-4$ meV: In Figure 7b, the half-width of the simulated peak is 19 meV, which is close to the experimental value of 21meV measured for an excitation energy of 1.998 eV in Figure 4b. This substantiates our choice $\sigma_{PL} \sim 2$ meV.

While for the $\langle d\rangle = 32$ Å sample we have measured $\bar{I}_{PL}$ by exciting *to the red* of the main absorption peak (i.e., $\epsilon_{excit} < E_{exciton} \cong 2.17$ eV, see vertical arrow in Figure 5), for the sample

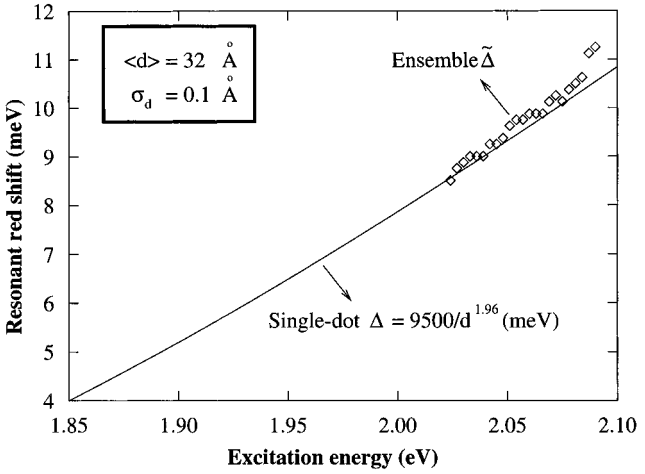

Figure 8. Simulated ensemble red shift $\tilde{\Delta}$ (diamond-shaped symbols) of $\langle d\rangle = 32$ Å, assuming a narrow size-distribution $\sigma_d = 0.1$ Å, compared with the underlying single-dot red shift Δ (solid line). Observe that the two functions start coinciding at $\epsilon_{excit} = E_g$ ($\langle d\rangle$).

with larger average size, $\langle d\rangle \cong 45$ Å, this would necessitate $\epsilon_{excit} < E_{exciton} \cong 1.86$ eV which is outside our laser range; therefore we had to excite the sample with $\langle d\rangle = 45$ Å by $\epsilon_{excit} = 1.83-2.0$ eV (Figure 5), i.e., mostly on the *blue side* of the main absorption peak. However, Figure 1 shows that at this excitation energy range, the ∼42 Å sample exhibits *two* absorption peaks (denoted "a" and "b"). Thus, this type red shift is no longer "resonant" and our analysis of eq 2 cannot be meaningfully applied to such a high excitation energy experiment. The raw data for the ensemble FLN of $\langle d\rangle = 45$ Å is shown in Figure 5.

Our simulation of the measured FLN spectra suggests a few observations:

(a) Figure 8 shows how the ensemble red shift $\tilde{\Delta}(\epsilon_{excit})$ (calculated with the parameters that fit the measured data of the $\langle d\rangle = 32$ Å sample) approach the single-dot red shift $\Delta(\epsilon_{excit})$ as the size distribution is artificially narrowed in the simulation ($\sigma_d \rightarrow 0$). We see that the ensemble and single-dot shifts coincide at a critical excitation energy $\epsilon_{excit} \sim E_g$ ($\langle d\rangle$).

(b) Figure 9a compares the measured ensemble red shift $\tilde{\Delta}(\epsilon_{excit})$ (diamondlike symbols) with the simulated result (crosses), in which all parameters (σ_{PL}, σ_d, $\langle d\rangle$, A, n) are held at the values that produced a fit to the data (Figure 6), except that now we set $\Delta(d) \equiv 0$ (compare with Figure 6 in which $\Delta \neq 0$). We see that even though the *intrinsic* red shift is taken as zero, the simulated *ensemble* red shift is nonzero. Clearly, a piece of the ensemble red shift is due to the existence of a size distribution and is unrelated to the spectroscopic characteristics of the individual dots. Figure 9 thus illustrates the importance of removing the spurious red shift $\tilde{\Delta}(\Delta = 0)$ from the measured one, before comparing the results with theory.

Figure 9b further shows the *difference* between the lines of Figure 9a, i.e.,

$$\delta(\epsilon_{excit}) = \tilde{\Delta}_{measured}(\epsilon_{excit}) - \tilde{\Delta}_{simulated}(\epsilon_{excit}; \Delta \equiv 0) \quad (8)$$

illustrating that this difference (diamondlike symbols in Figure 9b) is very close to the single-dot red shift deduced from experiment (line in Figure 9b, taken as eq 7). The fact that $\delta(\epsilon_{excit}) \cong \Delta(\epsilon_{excit})$ suggests a simple way to estimate $\Delta(\epsilon_{excit})$ i.e., use eq 8.

To understand why there is an ensemble red shift even in the absence of a microscopic, single-dot shift we show in Figure 10 the calculated ensemble emission spectra $\bar{I}(\epsilon_{excit})$ for two cases: In Figure 10b we use $\Delta(d) \neq 0$ (after eq 7), illustrating

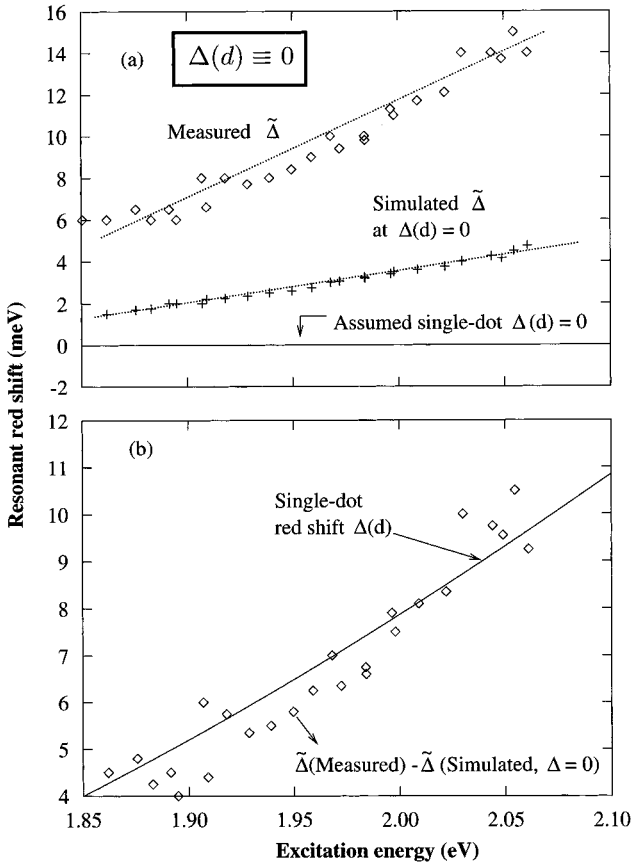

Figure 9. (a) Measured $\tilde{\Delta}_{measured}(\epsilon_{excit})$ ensemble red shift for $\langle d \rangle = 32$ Å (diamond-shaped symbols), compared with the simulated $\tilde{\Delta}_{simulated}(\epsilon_{excit}; \Delta \equiv 0)$ ensemble red shift (plus signs) assuming $\Delta(d) \equiv 0$. (b) The difference $\delta(\epsilon_{excit}) = \tilde{\Delta}_{measured} - \tilde{\Delta}_{simulated}$ ($\Delta = 0$) (diamond-shaped symbols) compared with the single-dot red shift $\Delta(d)$ of eq 7 (solid line).

how the individual, single-dot emission peaks a, b, and c produce the ensemble emission that is red-shifted with respect to the excitation energy (vertical line). If we now move the excitation energy to coincide with the emission peak of *one particular dot size* (peak a in Figure 10a, where $\Delta \equiv 0$), the *other* dots emit "out of resonance", so still $\Delta \neq 0$.

Figure 11 shows the simulated red shift for a few assumed average sizes $\langle d \rangle = 20$, 32 Å. We use $\sigma_d = 2.0$ and 2.5 Å, respectively. We see that $\tilde{\Delta}(\epsilon_{excit}, \langle d \rangle)$ *vs* ϵ_{excit} has an *increasing slope* as $\langle d \rangle$ increases, even though all of these curves have an identical underlying single-dot red shift $\Delta(d)$. Thus, even though the *single-dot* red shift *increases* as the dot size is reduced (eq 7), the *ensemble* red shift *decreases* as the dot size is reduced. This illustrates further that the measured ensemble red shift should not[8,9,11−13] be compared directly with a calculated $\Delta(d)$.

Finally, Figure 12 shows the single-dot red shift deduced from our experiments. This quantity should be directly compared to the prediction of theoretical models.

D. PL Lifetime. The PL lifetimes were measured in a sample of HF-treated InP QDs immobilized in a PVB film at 298 K and 13 K; the mean QD diameter was 30 Å. The PL decay as a function of time for this sample is shown in Figure 13; excitation was at 585 nm and the emission was monitored at 620 nm. The decay is multiexponential; the data were fit to three exponentials, and the results are presented in Table 1. At 298 K most of the decay (91%) can be described by two time constants of 28 and 73 ns; at 13 K most of the decay (98%) can be described by time constants of 173 and 590 ns.

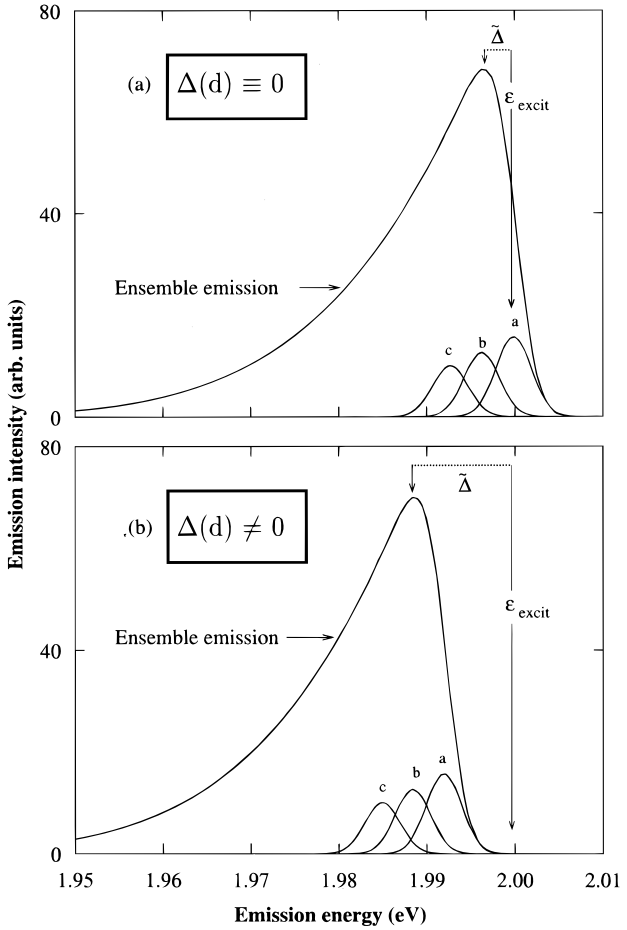

Figure 10. Simulated ensemble emission line shape $\bar{I}(\epsilon)$ for $\Delta(d) \equiv 0$ (part a) and for $\Delta(d) = 9500/d^{1.96}$ (part b). The curves labeled a, b, and c illustrate three single-dot emission lines $I(\epsilon)$. Curve a corresponds to the smallest dot in the ensemble. In part a the excitation energy coincides with peak a (so $\Delta = 0$), yet the ensemble red shift is nonzero.

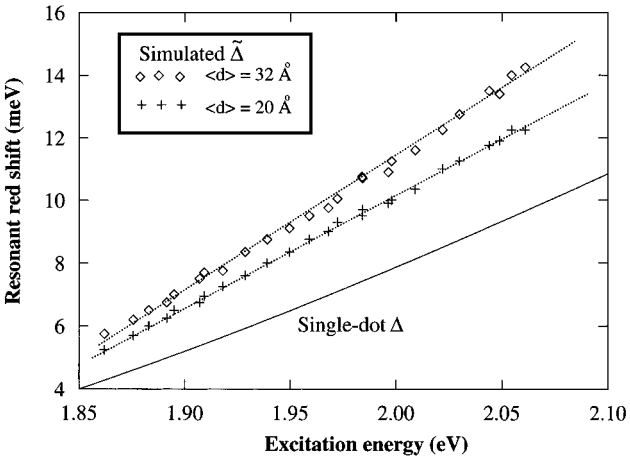

Figure 11. Simulated ensemble red shift $\tilde{\Delta}(\epsilon_{excit})$ for a few average sizes: $\langle d \rangle = 32$ Å; $\sigma_d = 2.5$ Å and $\langle d \rangle = 20$ Å; $\sigma_d = 2.0$ Å.

IV. Discussion

Our results show that for InP QDs formed via collodial chemical processes, very large effects due to a residual QD size distribution remain manifested in the photoluminescence spectroscopy of QD ensembles even after the colloidal samples have been subjected to size-selective precipitation techniques and size-selective photoexcitation. This behavior is similar to that reported for colloidal CdSe QD ensembles.[8−14]

When the colloidal samples are photoexcited well to the blue of the absorption onset, so that most of the QDs in the size

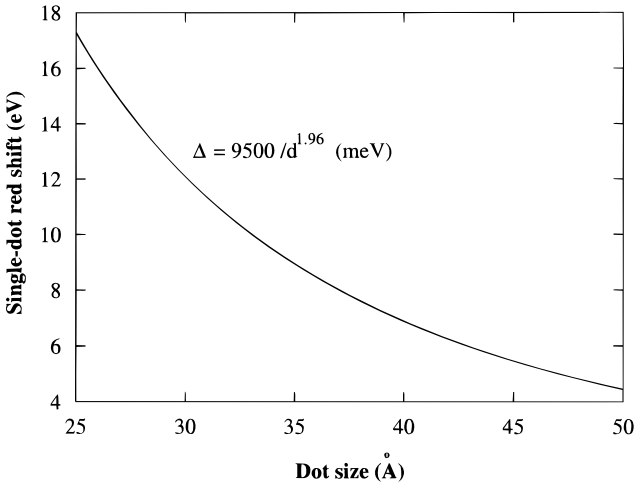

Figure 12. The single-dot red shift deduced from our experiments.

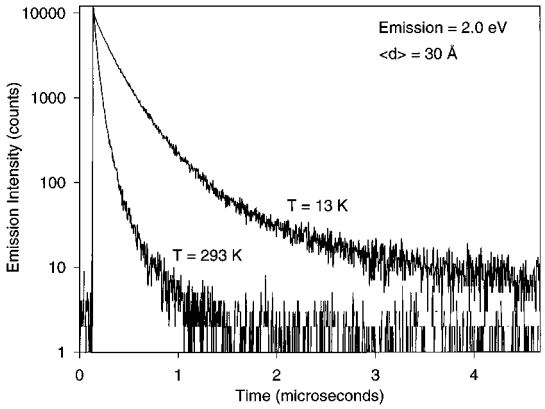

Figure 13. PL decay for HF-treated InP QDs at 298 K and 13 K.

TABLE 1: Multiexponential Fits of PL Lifetime (τ) for InP QDs with $\langle d \rangle = 30$ Å

temperature (K)	τ (ns)	contribution to decay, %
298	$\tau_1 = 28$	67
	$\tau_2 = 73$	24
	$\tau_3 = 166$	9
13	$\tau_1 = 6$	2
	$\tau_2 = 173$	78
	$\tau_3 = 590$	20

distribution are excited, the resulting global PL shows a very broad peak (line width of 175−225 meV) that is red-shifted by 100−300 meV from the first absorption peak (Figures 1, 2, and 3f). The broad PL line width is caused by inhomogeneous line broadening arising from the ∼10% size distribution sampled in the global PL experiment, as seen from the simulation (trace a in Figure 7). The large global red shift is caused by the volume dominance of the larger particles in the size distribution; the larger QDs will absorb most of the incident photons and will also show large red shifts since the PL excitation energy is well above their lowest transition energy.

As seen in Figures 3 and 4, the PL obtained by exciting into the red tail of the QD absorption spectrum, and thereby selectively exciting only the largest particles in the distribution, shows much smaller line widths (15−30 meV) and smaller red shifts compared to the global PL (compare Figures 2 and 5). However, as our analysis shows in Figures 6−12, even the size-selected PL/FLN spectra contain effects due to a residual size distribution. We have extracted the resonant red shifts for QDs of a single size from the experimental PL/FLN spectra using the approach described in Section III. The results of this analysis (see solid line in Figure 6 and Figure 12) show that the effective single-dot resonant red shift at 10 K exhibited by InP quantum dots that have been etched in HF to passivate surface states ranges from 4 meV for an excitation energy of 1.85 eV (corresponding to a QD size of 53 Å) to 9.7 meV for an excitation energy of 2.06 eV (corresponding to a QD size of 34 Å).

The origin of the resonant red shift in InP has been recently analyzed theoretically.[15,21] The methodology used was to treat a passivated quantum dot as a "giant molecule" in its own right, rather than an object drawn from an infinite crystal surrounded by an infinite potential barrier.[8,9,11−13] To this end, infinite-barrier **k•p** approaches[8,9,11−13] were avoided in favor of a pseudopotential super-cell approach,[15,21] in which a dot of any selected shape and size is modeled explicitly, and passivating atoms decorate all surface sites. To examine possible surface effects, cation-passivants and anion-passivants were selectively removed, and the electron structure was recalculated. Four possible models have been examined as to their ability to explain the resonant red shift: (1) emission from an intrinsic, spin-forbidden state, split from its singlet counterpart due to screened electron-hole exchange; (2) emission from an intrinsic, orbitally-forbidden conduction band state e.g., X_{1c} (rather than Γ_{1c}); (3) emission to an intrinsic, orbitally-forbidden valence band state (e.g., p-like); and (4) emission from extrinsic surface defects (e.g., surface vacancies). The experimental results reported here are quantitatively consistent with model 1 when the exchange interactions are screened by a distance-dependent[22] dielectric function[15] (see refs 23−25 for discussion of exchange screening). In model 1, an enhanced (relative to bulk) electron-hole exchange interaction splits the exciton state into a lower energy spin-forbidden state (triplet) and a higher energy spin-allowed singlet. Absorption occurs into the upper state, followed by relaxation to and emission from the lower state; the difference between these two states is the resonant red shift.[8−15] The value of the single-dot resonant red shift (as a function of QD size) derived from the experimental data is in excellent agreement with the theoretical predictions.[15]

Model 2 was rejected[15] because it was shown that the conduction band minimum in InP dots is not derived from an indirect X_{1c}-like state as in small GaAs particles,[15] and model 3 was rejected[15] because the symmetry of the envelope function of the valence band maximum was found to be 1s-like and not 1p-like as expected from simple **k•p** models. Model 4 shows that *fully* passivated QDs have no surface states, despite the large surface-to-volume ratio. However, in the event that some of the surface atoms were not capped by a passivant (due to, e.g., steric-hindrance by large passivating molecules), model 4 shows that surface *defect states* (due to surface uncapped In or surface uncapped *P*) could appear inside the QD band gap. These surface defects lead to large red shifts extending from one hundred to a few hundred meV depending on the surface conditions; such large red shifts are observed in unetched InP QDs but are removed upon HF etching.[18] The magnitude of the observed resonant red shifts reported here after etching is not consistent with the surface defects present in the initial QD synthesis; these are removed or passivated and do not affect the PL. While surface defect states do not explain the ≤10 meV *resonant* red shift, direct theoretical modeling of such states[15] show that they affect (i) the quantum-efficiency (through nonradiative recombination), and (ii) lead to a significant hybridization with the ordinary, corelike band edge states, thus affecting the radiative emission rate from theses states. Furthermore, since these hybridized states reflect the properties of the uncapped site (i.e., P or In "dangling bond") rather than those of the passivating molecules around this site, it was

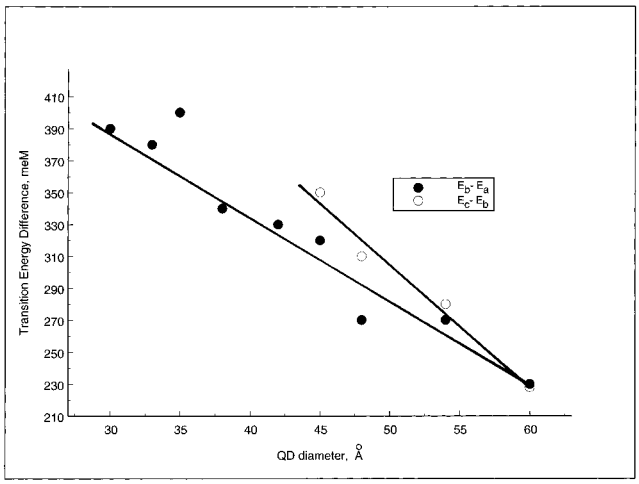

Figure 14. Energy spacings between the first and second absorption peaks (filled circles) and the second and third absorption peaks/shoulders (empty circles) as a function of QD diameter.

predicted[15] that surface defect states are mostly independent of the passivant and have size-dependent lifetimes. The degree of mixing of surface defect wavefunctions with the ordinary corelike band edge states remains unknown at this time.

The relatively long lifetimes of InP QDs with a mean diameter of 30 Å (ranging from 28−73 ns at 298 K and 173−590 ns at 13 K) are also consistent with model 1 since the spin-forbidden lowest excitonic state has a small probability for radiative transitions to the ground state.

Additional experiments which can be done for InP QDs to check the validity of model 1 include measuring the PL lifetime as a function of magnetic field,[8,9,12,13] measuring the intensity ratio of the zero phonon PL line to its replica as a function of magnetic field,[8] and measuring the degree of linear polarization of the PL.[12,13] In model 1: the PL lifetime should decrease with increasing magnetic field, the zero-phonon PL line intensity should increase relative to the one-phonon replica with magnetic field, and the degree of linear polarization should be negative. These experiments will be done in the future.

The absorption spectra of QDs with different diameters (Figure 1) show structure due to excited state transitions in the QDs. In Figure 1, the first excitonic peak is labeled a, while the second and third peaks or shoulders are labeled b and c; QDs with diameters ≥30 Å show a b feature, while QDs ≥ 42 Å show both b and c features. The energy spacing between the a and b and between the b and c peaks or shoulders in Figure 1 increase with decreasing QD size; this is the expected behavior for the quantized energy level spacings in QDs. The energy separations between peaks a and b and between b and c are plotted in Figure 14; for the former, the energy spacings range from 230 meV for 60 Å QDs to 400 meV for 30 Å QDs, while for the latter the spacings range form 230 meV for 60 Å dots to 350 meV for 45 Å dots. The global red shifts with respect to the higher energy transitions can be obtained by simply adding the energy spacings in Figure 14 to the red shifts in Figure 2.

The line widths of our FLN spectra are typically 15−30 meV; while these line widths are significantly narrower than the 175−225 meV line widths typically obtained from global (nonresonant) PL excitation, they are still much broader than line widths reported from PL measurements on single dots. For a variety of II−VI and III−V QDs, single-dot PL line widths have been reported to range from 40 to 1000 μeV.[26−31] The broader line widths in our FLN spectra are attributed to the significant QD size and shape distribution that still remains in the FLN experiment; this is evident in Figure 3 from the decreasing FLN line widths obtained as the excitation energy is moved to lower energies and hence to narrower QD size distributions (and also to larger QD diameters). Also, from Figure 1 it is seen that the absorption peak moves about 35 to 45 meV for every 1 Å change in QD diameter. Thus, the PL line width of 15−30 meV for our FLN spectra reflects a QD diameter variation of less than 1 Å! It is apparent that the PL line width is extremely sensitive to the spread in QD diameters, and that true line widths require PL data obtained from single dots. The experimental PL line widths observed for single QDs are smaller than the line widths we used in eq 3 by a factor of about 2 to 50. However, this does not affect the extracted red shifts we report here for single dots because the additional PL line broadening represented by $\sigma_{PL} = 2$ meV reflects a variation in the single-dot diameter of less than 0.1 Å.

The FLN spectra show a shoulder that is displaced from the highest energy PL peak by 30−35 meV; this is attributed to replicate PL lines caused by phonon emission. However, the bulk LO phonon energy for InP is 43 meV; further work is required to understand this difference.

V. Summary

In summary, we have found in this work that (i) the absorption spectra of our HF-etched and surface-passivated InP QDs exhibit up to three peaks or shoulders that reflect transitions to excited quantized states of the QDs; (ii) the near-edge PL emission shows a single broad peak (line width of 175−225 meV) when the excitation energy is well to the blue of the absorption onset (global PL); (iii) the global PL shows a red shift with respect to the first absorption peak that increases with decreasing QD size and ranges from about 300 to 100 meV as the mean QD diameter increases from 25 to 60 Å; (iv) the absorption and PL spectroscopic features both shift to the blue with decreasing QD size; (v) size-selective excitation into the red tail of the absorption onset produces much narrower PL peaks (15−30 meV) that become narrower with increasing excitation wavelength; (vi) size selective PL and PLE spectroscopy data has been analyzed to extract the resonant red shift as a function of a *single* QD diameter; (vii) the single QD resonant red shifts are much smaller than the global red shifts and increase with decreasing QD size (4 meV at 53 Å and 9.7 meV at 34 Å); (viii) the magnitude and QD size dependence of the single QD red shift is consistent with a model in which the emission occurs from an intrinsic, spin-forbidden state, split from its singlet counterpart due to screened electron-hole exchange; (ix) the line width of our narrowest size-selected PL peak is still much broader than PL line widths recently observed (40−1000 μeV) from *individual* III−V QDs. This is explained by the extreme sensitivity of the PL line width to variation in the QD diameter; a 15−30 meV PL line width reflects a variation of less than 1 Å in the QD diameters in the size-selected ensemble.

Acknowledgment. This work was funded by the U. S. Department of Energy, Office of Energy Research. O. I. Mićić, J. R. Sprague, and A. J. Nozik were supported by the Division of Chemical Sciences; H. M. Cheong, H. Fu, A. Mascarenhas, and A. Zunger were supported by the Division of Materials Sciences.

References and Notes

(1) O'Neil, M.; Marohn, J.; McLendon, G. *J. Phys. Chem.* **1990**, *94*, 4356.

(2) Eychmuller, J. A.; Hasselbrath, A.; Katsikas, L.; Weller, H. *Ber. Bunsenges Phys. Chem.* **1991**, *95*, 79.

(3) Hasselbarth, A.; Eychmuller, A.; Weller, H. *Chem. Phys. Lett.* **1993**, *203*, 271.
(4) Bawendi, M. G.; Carroll, P. J.; Wilson, W. L.; Brus, L. E. *J. Chem. Phys.* **1992**, *96*, 946.
(5) Nirmal, M.; Murray, C. B.; Bawendi, M. G. *Phys. Rev. B* **1994**, *50*, 2293.
(6) Petrova-Koch, V.; Muschik, T.; Kux, A.; Meyer, B. K.; Koch, F.; Lehmann, V. *Appl. Phys. Lett.* **1992**, *61*, 943.
(7) Hoheisel, W.; Colvin, Y. L.; Johnson, C. S.; Alivisatos, A. P. *J. Chem. Phys.* **1994**, *101*, 845.
(8) Nirmal, M.; Norris, D. J.; Kuno, M.; Bawendi, M. G.; Efros, A. L.; Rosen, M. *Phys. Rev. Lett.* **1995**, *75*, 3728.
(9) Efros, A. L.; Rosen, M.; Kuno, M.; Nirmal, M.; Norris, D. J.; Bawendi, M. *Phys. Rev. B* **1996**, *54*, 4843.
(10) Norris, D. J.; Bawendi, M. G. *Phys. Rev. B* **1996**, *53*, 16338.
(11) Norris, D. J.; Efros, A. L.; Rosen, M.; Bawendi, M. G. *Phys. Rev. B* **1996**, *53*, 16347.
(12) Chamarro, M.; Gourdon, C.; Lavallard, P.; Lublinskaya, O.; Ekimov, A. I. *Phys. Rev. B* **1996**, *53*, 1336.
(13) Chamarro, M.; Gourdon, C.; Lavallard, P. *J. Lumin* **1996**, *70*, 222.
(14) Woggon, U.; Gindele, F.; Wind, O.; Klingshirn, C. *Phys. Rev. B* **1996**, *54*, 1506.
(15) Fu, H.; Zunger, A. *Phys. Rev. B.* **1997**, in press.
(16) Mićić, O. I.; Curtis, C. J.; Sprague, J. R.; Jones, K. M.; Nozik, A. J. *J. Phys. Chem.* **1994**, *98*, 4966.
(17) Mićić, O. I.; Sprague, J. R.; Curtis, C. J.; Jones, K. M.; Machol, J. L.; Nozik, A. J. *J. Phys. Chem.* **1995**, *99*, 7754.
(18) Mićić, O. I.; Sprague, J. R.; Lu, Z.; Nozik, A. J. *Appl. Phys. Lett* **1996**, *68*, 3150.
(19) Guzelian, A. A.; Katari, J. E. B.; Kadavanich, A. V.; Banin, U.; Hamad, K.; Juban, E.; Alivisatos, A. P.; Wolters, R. H.; Arnold, C. C.; Heath, J. R. *J. Phys. Chem.* **1996**, *100*, 7212.
(20) Murray, C. B.; Norris, D. J.; Bawendi, M. G. *J. Am. Chem. Soc.* **1993**, *115*, 8706.
(21) Fu, H.; Zunger, A. *Phys. Rev. B* **1997**, *55*, 1642.
(22) Resta, A. *Phys. Rev. B.* **1977**, *16*, 2717.
(23) Takagahara, T.; Takeda, K. *Phys. Rev. B* **1996**, *53*, R4205. Takagahara, T. *Phys. Rev. B* **1993**, *47*, 4569.
(24) Bir, G. L.; Pikus, G. E. *Symmetry and Strain-induced Effects in Semiconductors*; Wiley: New York, 1975.
(25) Martin, E.; Delerue, C.; Allan, G.; Lannoo, M. *Phys. Rev. B* **1994**, *50*, 18258.
(26) Empedocles, S. A.; Norris, D. J.; Bawendi, M. G. *Am. Phys. Soc.* **1996**, *77*, 3873.
(27) Forchel, A.; Steffen, R.; Koch, T.; Michel, M.; Albrecht, M.; Reinecke, T. L. *Semicond. Sci. Technol.* **1996**, *11*, 1529.
(28) Gammon, D.; Snow, E. S.; Katzer, D. S. *Appl. Phys. Lett.* **1995**, *67*, 2391.
(29) Grundmann, M.; Christen, J.; Ledentsov, N. N.; Bohrer, J.; Bimberg, D.; Ruvimov, S. S.; Werner, P.; Richter, U.; Gosele, U.; Heydenreich, J.; Ustinov, V. M.; Egorov, A. Y.; Zhukov, A. E.; Kop'ev, P. S.; Zh.I., A. *Phys. Rev. Lett.* **1995**, *74*, 4043.
(30) Samuelson, L.; Carlsson, N.; Castrillo, P.; Gustafsson, A.; Hessman, D.; Lindahl, J.; Montelius, L.; Petersson, A.; Pistol, M.-E.; Seifert, W. *Jpn. J. Appl. Phys.* **1995**, *34*, 4392.
(31) Nagamune, Y.; Watabe, H.; Nishioka, M.; Arakawa, Y. *Appl. Phys. Lett.* **1995**, *67*, 3257.